Available online at www.sciencedirect.com
SCIENCE DIRECT
Journal of Power Sources 158 (2006) 464–476
JOURNAL OF POWER SOURCES
www.elsevier.com/locate/jpowsour

Ni and Ni–Mo hydrogen evolution electrocatalysts electrodeposited in a polyaniline matrix

Alexis Damian, Sasha Omanovic *

Department of Chemical Engineering and McGill Institute for Advance Materials, McGill University, 3610 University St., Montreal, Que., Canada H3A 2B2

Received 8 August 2005; received in revised form 2 September 2005; accepted 6 September 2005
Available online 19 October 2005

Abstract

Electrocatalytic activity of Ni and NiMo electrodeposited in a three-dimensional polyaniline (PANI) matrix was investigated in the hydrogen evolution reaction (HER). By using PANI an increase in surface roughness of the metallic catalytic layers could be obtained, ultimately yielding an increased overall electrocatalytic activity in the HER. It was demonstrated that alloying Ni with Mo results in an increased electrocatalytic activity in the HER when compared to pure Ni. This is due to an improved intrinsic activity of the material, which was explained on the basis of the modification of the electron density in the d-shell upon alloying Ni with Mo. An improvement of the NiMo/PANI catalysts' intrinsic properties was also demonstrated by a significant decrease in activation energy in the HER when compared to the Ni/PANI layer. By using DC linear polarization and AC electrochemical impedance spectroscopy techniques the mechanism and kinetics of the HER on the investigated catalysts was determined.

Keywords: Hydrogen; Water electrolysis; Electrocatalysis; Nickel; Molybdenum; Polyaniline

1. Introduction

It has been obvious that one of the major problems of today's world is in its heavy dependency on fossil fuels. This, in turn, creates a range of socio-economical, geopolitical, and environmental problems. The utilization of fossil fuels, especially oil, is predicted to increase exponentially in the coming years, while at the same time their availability will decrease. Consequently, this will contribute to a further increase of the above problems. The only solution to these problems is to increase the use of sustainable energy resources. Since hydrogen, the most abundant element on earth, is the cleanest and ideal fuel (carrier), it has been increasingly considered as the *fuel of the future* [1–4]. Although production of hydrogen by water electrolysis is not currently cost-competitive to natural gas reforming, it represents a process where hydrogen can be produced by *true renewable* and fully *environmentally friendly* energy sources (solar, wind, hydro), without co-production of the green-house gas, CO_2. Industrial water electrolysis is, for the time, being carried out using a liquid alkaline electrolyte. However, due to a range of disadvantages of this technology, the use of solid polymer electrolyte membrane (PEM)-type generators (the technology very similar to the PEM fuel cell technology) with demineralized water as the raw material offers a viable alternative, especially for residential and small scale applications. Although the inherent advantages of the PEM technology over the alkaline one are clearly established (greater safety and reliability, higher differential pressures, higher operating current densities and efficiency, rapid transient responses, construction simplicity and maintenance, etc.), one of the main obstacles associated with the large-scale commercial application of the PEM hydrogen generator is related to high investment costs. This is mainly due to the use of noble metals (Pt, Ir, Ru) as electroactive catalyst materials at high loadings [5,6]. It has been recently shown [7] that the major portion of the cost of the hydrogen infrastructure based on the use of wind turbines (in northern Germany) is related to the hydrogen generator (water electrolyser). In the same study, the authors have shown that the cost of the hydrogen gas produced by wind-powered water electrolysis and used to fuel a passenger car is still twice the cost of diesel fuel in Germany (normalized with respect to the

* Corresponding author. Tel.: +1 514 398 4273; fax: +1 514 398 6678.
E-mail address: sasha.omanovic@mcgill.ca (S. Omanovic).

0378-7753/$ – see front matter © 2005 Elsevier B.V. All rights reserved.
doi:10.1016/j.jpowsour.2005.09.007

mileage). However, due to the rapidly increasing cost of oil, the authors predict that the situation will become opposite in the near future. Therefore, there is a great need to develop a more active, efficient, stable, and cheap electrocatalyst for water splitting in the PEM hydrogen generator that would offer low overpotentials for the hydrogen evolution reaction (HER) at rather high current densities (1–2 A cm^{-2}), and ultimately lower the cost of produced hydrogen.

Three properties play an important role in selecting catalytically active materials for the HER: (a) an actual *intrinsic* electrocatalytic effect of the material, (b) a large active surface area per unit volume ratio, both of which are directly related to the (over)potential used to operate the electrolyser at significant current densities, and (c) catalyst stability. Consequently, an approach used in the design of good HER electrocatalysts is based either on the increase of the active surface area of the electrode (catalyst) [8–11] and/or on the design of an electrode material having high intrinsic catalytic activity [12–16], both of which result in a decrease in the HER overpotential. Several attempts have been made to explain the characteristics of the HER overpotential of individual metals using various physical and/or electronic parameters, including the atomic number [12], the work function [13], the bond-strength of metals [14], the heat of adsorption of hydrogen on metals [15], and the electronegativity [16]. We have shown [17] that by alloying nickel with left transition metals (W, Mo, Fe), an increase in the intrinsic electrocatalytic activity in the HER, compared to pure nickel, can be obtained. In general, it has been concluded that the intrinsic catalytic activity for the HER can be related to the electronic structure of metals [17–21], although a well-known 'spillover' effect in heterogeneous catalysis has also been used to interpret the synergism of transition metal-based HER alloys [22].

The present work discusses results on the use of conducting polymer polyaniline (PANI) as a support/matrix/template for the construction of Ni and NiMo hydrogen evolution catalyst layers on an inert electrode substrate (glassy carbon). The aim of the work was to investigate the effect of PANI on the resulting catalyst surface roughness, and also to achieve an increase in intrinsic electrocatalytic activity in the HER by alloying Ni with Mo. Nickel and NiMo have been chosen as catalytic materials due to their high intrinsic activity in the HER and their low cost compared to noble metals currently used in the construction of PEM hydrogen generators. PANI has been chosen due to its (i) insulating properties in the cathodic region relevant for hydrogen production, thus avoiding their catalytic interference with the HER charge transfer process and Ni and NiMo catalysts, (ii) favorable pattering morphology, (iii) stability in the PEM environment of a hydrogen generator (low pH), (iv) high solubility in aqueous solutions, (v) well-developed and simple electrochemical polymerization methodology, and (vi) suitability for potential commercial use. Although electrocatalysis on conducting polymer-based layers incorporating metal particles (mostly Pt or other noble metals) has been reported in literature, the majority of the work is related to oxidation reactions [23–28], while reduction reactions have been much less studied, and are mainly concentrated in the area of oxygen reduction [29–32]. To the best of our knowledge, only a few publications discussing the use of conducting polymers in hydrogen reduction (production) have been reported [33–36]. In [35], no metal particles were incorporated into the polypyrrole film but the HER actually took place at the substrate (iron) surface. In reference [36], electroless nickel was used as a catalyst incorporated into a polypyrrole film but the substrate chosen was platinum. However, the actual catalytic effect of incorporated nickel particles in the HER was difficult to distinguish from the catalytic effect of the Pt substrate due to the porosity of the polymer layer, as studied in [37]. In the present work, we used a glassy carbon (GC) substrate, which is inactive in the HER in the potential region of interest, which allowed us to investigate only an effect of the catalytic materials, Ni and NiMo, on the mechanisms and kinetics of the HER.

2. Experimental

The electrocatalytic activity of Ni/PANI and NiMo/PANI layers in the hydrogen evolution reaction (HER) was studied in 0.5 M H_2SO_4 solution for a wide temperature range, from 295 K to 338 K. Chemicals used for the research were purchased from Sigma–Aldrich Company and Fisher Scientifics, and were used without further purification. All solutions were prepared using nanopure water of resistivity 18 MΩ cm. All measurements were made in an oxygen-free solution, which was achieved by continuous purging of the cell electrolyte with argon gas (99.998% pure).

A standard three-electrode, two compartment cell was used in all experiments. The counter electrode was a large-area platinum electrode of high purity (99.99%, Alfa Aesar), which was degreased by refluxing in acetone, sealed in soft glass, electrochemically cleaned by potential cycling in 0.5 M sulfuric acid, and stored in 98% sulfuric acid. During measurements, the counter electrode was separated from the main cell compartment by a glass frit. The reference electrode was a commercially available mercury/mercurous sulfate electrode (MSE). The working electrode was a PANI-based catalytic layer deposited on a glassy carbon (GC) substrate of surface area 0.17 cm^2. GC was chosen as a substrate material since it has very large overpotential for hydrogen evolution, thus offering a wide potential region for the investigation of the HER without substrate interference. The GC electrode (substrate) was made of a rectangular piece of GC sealed in an epoxy, thus giving a two-dimensional surface area available for the electrodeposition of an electrocatalytic layer. Before electrodeposition of a nickel_based-conducting polymer (Ni_B/CP) layer, the GC substrate was carefully prepared by mechanical wet-polishing using #600 and #1500 grit sand paper, followed by thorough rinsing with distilled water and cleaning in an ultrasonic bath for 5 min in order to remove polishing residues. Subsequently, the substrate was degreased with ethanol, rinsed with nanopure water, and further electrochemically cleaned (activated) in 0.5 M H_2SO_4 by potentiodynamic cycling between the hydrogen and oxygen evolution potential. The formation of active PANI-based catalytic layers was done by potentiostatic electrodeposition of Ni or NiMo on a PANI layer pre-deposited on the GC substrate. The experimen-

Table 1
Experimental conditions used in formation of Ni/CP and NiMo/CP layers on a GC substrate

Layer	Bath composition		Ni/CP-layer formation conditions
Polyaniline	Aniline	0.05 M	Deposition potential: 0.82 V_{SCE}; deposition time: 5 min
	H_2SO_4	0.5 M	
Ni	$NiSO_4{\cdot}6H_2O$	52.1 g L^{-1}	Deposition potential: −1.45 V_{SCE}; deposition time: 5 min
	H_3BO_3	6.2 g L^{-1}	
	H_2SO_4	To adjust pH	
	pH	3	
Ni_2Mo	$NiSO_4{\cdot}6H_2O$	52.1 g L^{-1}	Deposition potential: −1.45 V_{SCE}; deposition time: 5 min
	$Na_2MoO_4{\cdot}2H_2O$	72.9 g L^{-1}	
	$Na_3C_6H_5O_7{\cdot}2H_2O$	88 g L^{-1}	
	NH_4OH	Excess	
	pH	10.4	
Ni_6Mo	$NiSO_4{\cdot}6H_2O$	79 g L^{-1}	Deposition potential: −1.45 V_{SCE}; deposition time: 5 min
	$Na_2MoO_4{\cdot}2H_2O$	48 g L^{-1}	
	$Na_3C_6H_5O_7{\cdot}2H_2O$	88 g L^{-1}	
	NH_4OH	Excess	
	pH	10.4	

tal conditions and bath compositions are presented in Table 1. A control catalyst (Ni electrodeposited on a copper substrate, Ni/Cu) was prepared according to the procedure described in [17]. After the formation of each electrode layer, the electrode surface was carefully rinsed with large amounts of nanopure water in order to remove any residues of bath chemicals and unattached catalyst particles. Then the electrode was placed in the electrochemical cell, and in order to reduce any nickel oxides spontaneously formed on the catalyst surface, i.e. to activate the electrocatalyst, the electrode was polarized at −1.15 V (versus MSE) for 5 min, followed by stabilization at open-circuit-potential (OCP) until a steady-state OCP value was obtained (usually less than 5 min). Then, a linear polarization measurement was made, starting from the OCP to potential OPC-500 mV, at a scan rate of 0.5 mV s^{-1}. The DC polarization measurement was followed by a set of electrochemical impedance spectroscopy (EIS) measurements at selected overpotentials in the potential region between OCP and OCP-500 mV. An Autolab PGSTAT 30 potentiostat/galvanostat/frequency-response-analyzer was used in all the electrochemical measurements, while the scanning electron microscopy (SEM) analysis was done using a Hitachi 4700 field emission SEM. All the DC polarization curves were corrected for the IR-drop.

To determine the chemical composition of a NiMo catalyst, an ICP technique was employed using a Thermo Jarell Ash Trace Scan inductively coupled-plasma (ICP) spectrometer. Metallic catalytic layers were dissolved in 10 mL of boiling aqua regia (water, concentrated nitric acid and concentrated hydrochloric acid in a 1:1:3 volume ratio). Solutions of 50 and 100 ppm were prepared from Ni, and Mo standard solutions (Fisher ICP standards, 1000 μg mL^{-1}) to determine a calibration curve. Three measurements were run for each sample. The exact compositions of the two NiMo catalysts used in research are presented in Table 1.

3. Results and discussion

3.1. Morphology of PANI, Ni/PANI, and NiMo/PANI

As mentioned in the introduction, the aim of using the conducting polymer polyaniline (PANI) as a three-dimensional (3D) matrix for electrodeposition of Ni and NiMo was to investigate its influence on the surface roughness of the resulting electrodeposited metallic catalyst layers. Morphology of a PANI layer deposited on a glassy carbon (GC) substrate was first characterized using scanning electron microscopy (SEM) (Fig. 1a). The micrograph shows a highly fibrilar, branched, and porous structure of the PANI layer, with an average thickness of fibers of ca. 100 nm. Since the PANI layer is not conducting in the potential region of Ni and Mo electrodeposition, it was hypothesized that its role would be to serve only as an inert structuring template that would prevent formation of a compact metallic layer of a two-dimensional (2D) morphology, and preferably control the growth of the metal phase in a way to achieve at least a quazi-3D morphology. Fig. 1b shows an image of a catalyst layer produced by electrodeposition of Ni on a pre-deposited PANI layer. As comparison, a Ni layer electrodeposited on a Cu substrate in the absence of PANI is shown in Fig. 1c (control catalyst). The difference in the morphology between the two layers is substantial. While the Ni-control layer displays a compact structure and semi-2D morphology, the Ni/PANI electrode is covered by a sub-monolayer of spherical Ni particles having an average diameter of 3 μm. The image shows the presence of only traces of PANI residues attached to Ni particles, i.e. an absence of a continuous PANI phase can be observed. At longer deposition times, the Ni layer grows to a thickness of at least three mono-spherical layers (Fig. 1d), offering a highly porous and defined 3D structure. Considering the fibrous morphology of the PANI layer presented in Fig. 1a, it is quite surprising to see the globular-like structure of the produced Ni layer. At the moment,

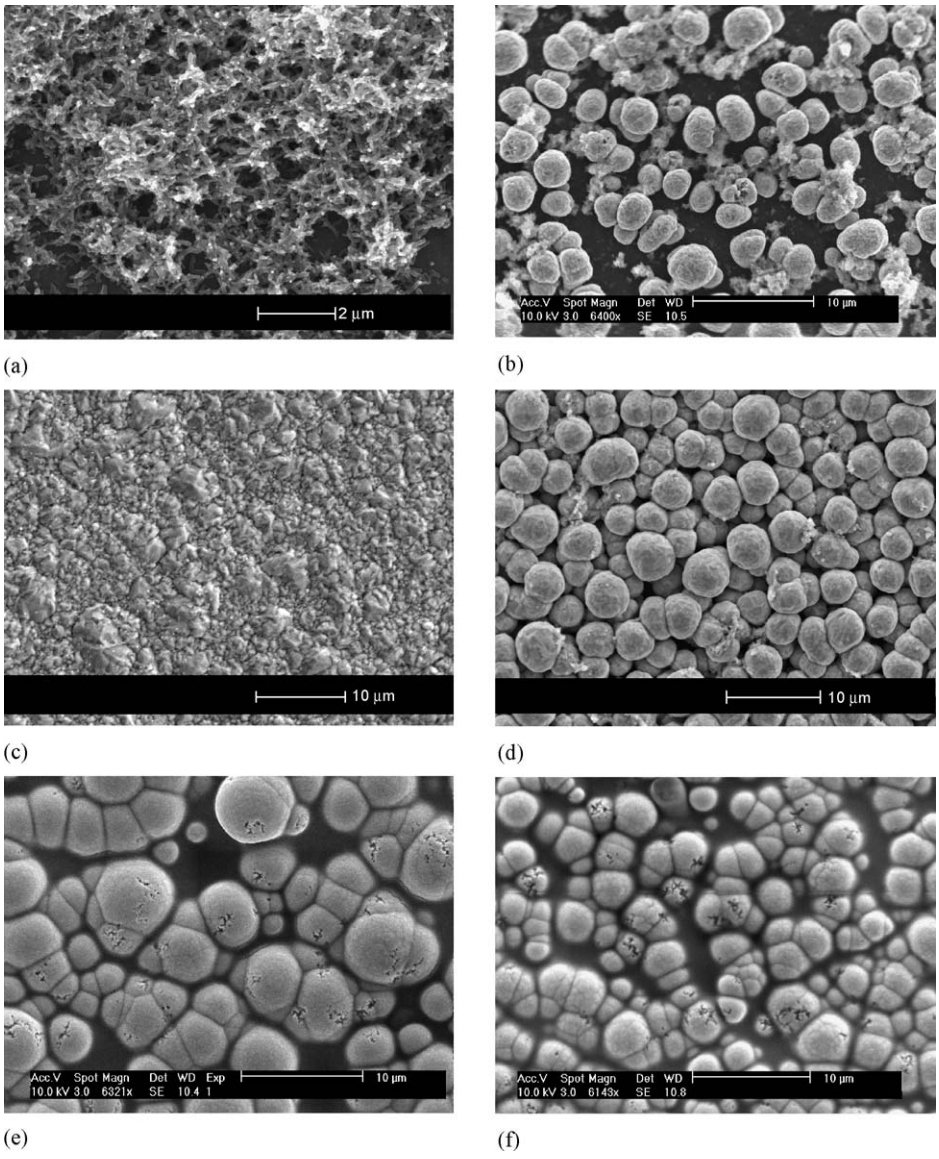

Fig. 1. SEM images showing a surface morphology of (a) polyaniline (PANI) electrodeposited on a GC substrate, and electrodes made by electrodeposition of Ni at (b) short, 5 min, and (d) long, 20 min times, and (e) Ni_6Mo and (f) Ni_2Mo at short times on a PANI layer pre-deposited on a GC substrate. (c) Morphology of a Ni-control catalyst.

it is not clear what could be a fundamental reason for such a large difference in the observed structure/morphology transformation, but the influence of hydrophobic, structural (fibrous) or surface charge distribution properties of the PANI layer could be one of the possible effects.

Fig. 1e and f show that the morphology of the two NiMo/PANI layers is different than the morphology of the Ni/PANI layer (Fig. 1b and d). SEM micrographs Fig. 1e and f reveal the presence of both the metallic and polymer phases on the GC surface. The NiMo phase is composed of globular/cauliflower-like particles with sizes ranging from ca. 2 μm to 8 μm on the Ni_6Mo/PANI surface (Fig. 1e), and ca. 1 μm to 5 μm on the Ni_2Mo/PANI surface (Fig. 1f). The micrographs demonstrate that the Ni_2Mo/PANI surface offers a narrower particle size distribution than the Ni_6Mo/PANI surface. It can also be observed on both micrographs that some smaller ellipsoid-shaped globules appear on top of the larger globules. The borders of both the smaller and bigger globules (particles) are circular or quazi-circular, and unlike the situation on the Ni/PANI surface (Fig. 1b and d) the particles are mostly merged together. The difference in the particle size distribution between the two NiMo catalysts (Fig. 1e and f) indicates that lower Ni content in the alloy results in a higher surface roughness. Also, comparing the three layers formed at the same deposition time (Fig. 1b, e, and f) it appears that both bimetallic NiMo/PANI layers offer a higher surface coverage than the Ni/PANI layer. Both these observations were also confirmed by EIS measurements, discussed later in the paper (Table 3).

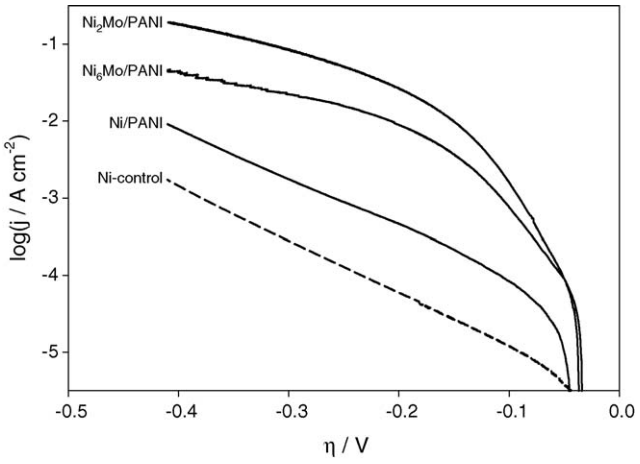

Fig. 2. Linear Tafel polarization curves recorded on PANI-based electrocatalysts (solid lines). The dashed line represents a response of a control catalyst, Ni-control. The curves were corrected for the IR-drop; scan rate = 0.5 mV s^{-1}.

3.2. DC linear Tafel polarization

In order to investigate the electrocatalytic activity of the prepared catalytic layers, Tafel linear polarization measurements were made, and the corresponding electrochemical parameters (Tafel slope, exchange current density, transfer coefficient) were derived from the recorded curves. Fig. 2 shows a set of Tafel curves recorded in 0.5 M H_2SO_4 on all the catalyst layers investigated, together with a control curve (dashed line) recorded on the control Ni catalyst (Fig. 1c). The curves were corrected with respect to a reversible HER potential at the given conditions ($E_{rev} = -0.015$ V versus standard-hydrogen-electrode, SHE in 0.5 M H_2SO_4, pH 0.25) and for the IR-drop. The Tafel curve recorded for the Ni/PANI layer (Fig. 2) shows a classical Tafelian behavior, clearly indicating that the HER on Ni/PANI is a purely kinetically controlled reaction described by the Tafel equation [17,38] $\eta = a + b \log j$, where η (V) represents the applied overpotential, j (A cm^{-2}) the resulting (measured) current density, b (V $decade^{-1}$) the Tafel slope, and a (V) is the intercept related to the exchange current density j_0 (A cm^{-2}) through equation $a = (2.3RT)/(\beta nF) \times \log j_0$. The other parameter of interest is β, the symmetry factor, which can be calculated from the Tafel slope as $b = -(2.3RT)/(\beta nF)$, and n represents the number of electrons exchanged, F (=96,485 C mol^{-1}) is the Faraday constant, and R (=8.314 J mol^{-1} K^{-1}) is the gas constant. Since the Ni/PANI curve in Fig. 2 does not show any significant change in the Tafel slope, the same HER reaction mechanism should be valid through the entire overpotential region investigated. The value of the Tafel slope determined from the curve is 156 mV $decade^{-1}$. According to the general HER mechanism in acidic media [38–40], this value indicates that the Volmer reaction step, i.e. adsorption of hydrogen on nickel to form $Ni–H_{ads}$ ($Ni + H^+ + e^- \leftrightarrow Ni–H_{ads}$), is the rate determining step (rds). The corresponding values of the transfer coefficient and exchange current density are 0.38 and 27 μA cm^{-2}, respectively (Table 2). Note that for the Volmer step the symmetry factor, β, is equal to the transfer coefficient, α (i.e. $\alpha = \beta$), while for the Heyrovsky step, i.e. desorption of adsorbed hydrogen to form molecular hydrogen ($Ni–H_{ads} + H^+ + e^- \leftrightarrow H_2 + Ni$) the transfer coefficient is equal to $\alpha = 1 + \beta$ [22,38]. From Table 2 it could also be noticed that the measured Tafel slope and transfer coefficient values for Ni/PANI deviate from the theoretical values, 116 mV $decade^{-1}$ and 0.5, respectively [38–40]. This phenomenon has already been reported in the literature [17,38] and has been explained by the presence of a thin oxide film on the catalyst's surface [41–43]. From the above discussion, one can conclude that a higher value of the transfer coefficient, which is often used as a comparison parameter, indicates a better intrinsic electrocatalytic activity of the material. Very similar values of the Tafel slope and transfer coefficient were obtained on a Ni-control catalyst (Table 2). However, Fig. 2 shows that at overpotentials below −0.1 V, the Ni/PANI catalyst offers ca. 800% higher overall electrocatalytic activity than the Ni-control. Also, the relative electrocatalytic activity at zero overpotential (equilibrium condition), i.e. the exchange current density value obtained on a Ni/PANI catalyst, is an order of magnitude (1000%) higher than on Ni-control. Although in both cases the same catalytic material was used (Ni), SEM and EIS measurements revealed that the increased electrocatalytic activity of the Ni/PANI catalyst is a consequence of both an increased surface area and a higher intrinsic activity of Ni/PANI relative to Ni-control. A contribution of the increased surface area could be clearly seen on the micrographs presented in Fig. 1c and d, which show that the 3D Ni/PANI surface offers a considerably higher surface area (roughness) than the 2D Ni-control surface. On the other hand, the increased intrinsic activity could be due to an increased number of electroactive surface sites formed when a Ni layer is electrodeposited in the presence of PANI. This point will be discussed in more detail later in the text.

In contrast to pure Ni, the polarization curves recorded on the bicomponent electrocatalysts, Ni_2Mo/PANI and Ni_6Mo/PANI (Fig. 2), display two potential-dependent regions related to the HER. At low overpotentials (greater than −150 mV), the curves

Table 2
HER kinetic parameters (b, j_0) obtained by analysis of the curves presented in Fig. 2. The table also shows the data used to compare the electrocatalytic activity of the investigated coatings in terms of (a) overpotential needed for a fixed hydrogen production rate determined by a current density of 1 mA cm^{-2}, and (b) the resulted production rate at a fixed energy input (fixed overpotential of −150 mV). Results for a control-catalyst (Ni-control) are also presented for comparison

Catalyst	b (mV $decade^{-1}$)	j_0 (μA cm^{-2})	α	η (mV) at 1 mA cm^{-2}	j (μA cm^{-2}) at −150 mV
Ni-control	147	−2.6	0.39	−379	−27
Ni/PANI	156	−27	0.38	−259	−215
Ni_2Mo/PANI	40	−5.4	1.45	−91	−9800
Ni_6Mo/PANI	55	−11.2	1.06	−107	−3700

are characterized by a well-defined Tafelian behavior (Region I), while at higher overpotentials (less than −200 mV) a significant deviation from the low-overpotential Tafelian behavior was recorded (Region II), i.e. there is a significant change in the Tafel slope. The deviation from the Tafelian behavior at high overpotentials or even the existence of two Tafel regions has already been reported in the literature [22,44–50] for similar HER electrocatalytic materials, and a number of explanations have been given. A change in the HER reaction mechanism, i.e. a transition from the Heyrovsky to the Volmer rds [22], has been suggested as one possible explanation. The fundamental reason for this transition could be related to the depletion of the d-electron density at the Fermi level of the NiMo alloys by adsorbed hydrogen [51], which remains partially uncompensated at lower overpotentials. However, by cathodic polarization to higher overpotentials, the d-electron density at the Fermi level increases, which then enhances the kinetics of the Heyrovsky step, and consequently the Volmer step becomes the rds at high overpotentials. Mass-transport limitations through narrow pores on the catalyst surface [47], or a decrease in the active surface area [46,48,49] have also been suggested as possible reasons for the observed diffusion-like shapes of the Tafel curves. However, our EIS analysis did not show the existence of mass-transport limitations and surface blockage of the NiMo/PANI layers, and these two possibilities could be eliminated as explanations for the observed Tafel slope change, as well as an IR-drop influence [48] since all the Tafel curves in Fig. 2 were corrected for the IR-drop. A decrease in Tafel slope at very high overpotentials could also be related to formation of hydrides in the outer region of the surface layer [22,44,52]. By polarization of the two NiMo/PANI bimetallic layers at high overpotentials, a large amount of atomic and molecular hydrogen is generated. This hydrogen is then absorbed into the metallic catalyst layer close to the electrolyte interface. The strong bonding between metal and absorbed hydrogen atoms becomes a barrier to hydrogen evolution, due to the modification of the electronic and structural properties of the metallic catalyst layer in the near-surface region. This, in turn, results in an increase in the Tafel slope and hydrogen overpotential at high current densities. Due to the electron-donor character of hydrogen, by going from the right-hand side transition metals with almost-filled d-orbitals (e.g. Ni) to the left-hand side metals with half-filled or almost-empty d-orbitals (e.g. Mo, W, V, Ti) the binding energy for an M–H bond increases [15], and thus the metal's ability to form corresponding hydrides. Hence, it can be expected that the two bimetallic layers used here (Ni_2Mo/PANI and Ni_6Mo/PANI) are more susceptible to hydride formation than pure nickel. This susceptibility increases with an increase in cathodic (over)potential. Hence, considering all the possibilities discussed above, it appears that the formation of hydrides at high overpotentials is the major reason for the observed Tafel slope change. In addition, the change in the d-electron density and subsequent influence on the kinetics of the Heyrovsky reaction step can also be a contributing factor.

The polarization curves in Fig. 2 yield Tafel slope and transfer coefficient values of 40 mV decade^{-1} and 55 mV decade^{-1}, and 1.45 and 1.06, for the Ni_2Mo/PANI and Ni_6Mo/PANI layers, respectively (Table 2). Similar values were also obtained on sputter-deposited NiMo and NiW electrodes in a highly basic medium [45] and NiMo electrodes prepared by arc-melting [22] in a highly acidic medium. Hence, it appears that the Heyrovsky desorption controls the HER kinetics on the two NiMo/PANI catalysts at low overpotentials, while the Volmer step then proceeds at a significant rate [38–40]. Considering the exchange current density values, j_0, presented in Table 2, one could see that at equilibrium (zero overpotential) both NiMo/PANI layers offer a lower electrocatalytic activity than the Ni/PANI layer. However, although a value of exchange current density is very frequently used for the characterization of electrocatalytic activity, it has been reported that values of Tafel slope and transfer coefficient in the low overpotential region (Region I) are as, or even more important than a favorable exchange current density value, j_0 [44]. This is due to the fact that the HER reaction does not occur at a reversible potential (i.e. zero overpotential), but a certain overpotential is required for the reaction to proceed at a measurable rate. Hence, in order to compare the electrocatalytic activity of the catalysts in Fig. 2 at the conditions relevant for the operation of a hydrogen generator, one can fix current density (i.e. hydrogen production rate) and compare the resulting overpotentials required to reach the given current density value. This would give an indication on the amount of energy (overpotential) that should be invested to produce a specified amount of hydrogen (since the current is, through the Faraday law, directly related to the amount of produced hydrogen). Overpotential values for each catalyst, measured at current density of 1 mA cm^{-2}, are presented in Table 2. It is obvious that Ni-control requires the largest energy input (overpotential) for the given hydrogen production rate, −379 mV, while Ni_2Mo/PANI requires the lowest energy input, −91 mV. Considering that power density is a product of the applied current density and the resulting overpotential, this represents energy saving of ca. 76% with respect to the control catalyst. Another common way of comparing the electrocatalytic activity of HER electrocatalysts is to fix the overpotential (energy input) and then compare the resulting current density values, i.e. the amount of hydrogen that would be produced by each catalyst. The results for an overpotential of −150 mV (which is in the overpotential range expected for a hydrogen generator operation) are presented in Table 2. Again, similarly to the behavior obtained at a fixed current density, Ni_2Mo/PANI yields the best electrocatalytic activity. The amount of hydrogen that could be produced using Ni_2Mo/PANI is ca. 360 times larger than if Ni-control were used.

The information obtained from the Tafel polarization data demonstrates that all the investigated PANI-based catalysts are very active in the HER, showing a superior *overall* catalytic activity over a Ni-control catalyst. Ni_2Mo/PANI showed to be the best overall catalyst. However, since the Tafel curves presented in Fig. 2 are normalized to the *geometric* area of the catalyst and not to the *real electrochemical* area, the results discussed above cannot offer a definite conclusion if the observed electrocatalytic activity is a result of only an increased surface area of the catalysts, or if an improvement in the intrinsic (electronic) electrocatalytic properties of the catalyst material is also a contributing factor. Therefore, in order to obtain information

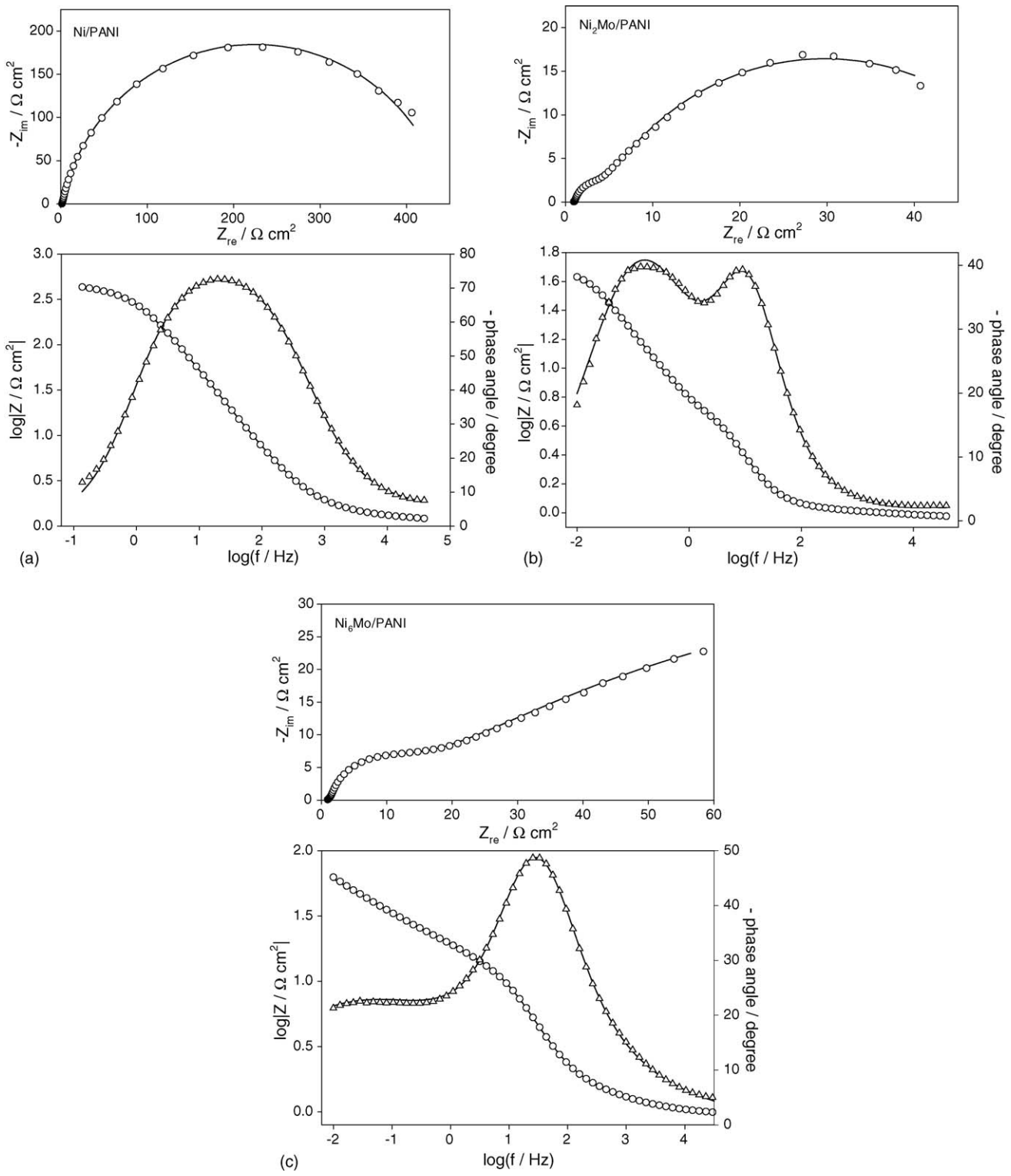

Fig. 3. (a) Nyquist and Bode plot showing an EIS response of a Ni/PANI electrode at overpotential −65 mV. (b) Nyquist and Bode plot showing an EIS response of a Ni_2Mo/PANI electrode at overpotential −65 mV. (c) Nyquist and Bode plot showing an EIS response of a Ni_6Mo/PANI electrode at overpotential −65 mV. Symbols are experimental and solid lines are modeled data.

on the intrinsic activity of the investigated layers in the HER, the curves presented in Fig. 2 should be normalized to the real electrochemically active surface area. An EIS technique has been proposed as the most appropriate technique that can be used for the real surface area determination in electrochemical systems [17,44]. Thus, the following section of the paper will discuss the EIS results obtained on all the catalytic layers used. A real electrochemically active surface area and the corresponding intrinsic activity of each catalyst will be subsequently determined. In addition, although the SEM and DC Tafel polarization tech-

niques gave information on the morphology and *overall* electrocatalytic activity of the PANI-based electrolytic layers studied, respectively, these techniques cannot provide information on the structure of the electrode/electrolyte interface in terms of surface charge and electroactive centers distribution, hydrogen adsorption, and number of electrocatalytically active centres (i.e. the real surface area that is active in the HER). However, as it will be shown, this information can be conveniently obtained by using electrochemical impedance spectroscopy (EIS).

3.3. Electrochemical impedance spectroscopy

To ensure a complete characterization of the electrode/electrolyte interface and corresponding processes, EIS measurements were made over six frequency decades, from 50 kHz to 10 mHz, at selected overpotentials ranging from OCP to OCP-500 mV. Fig. 3a–c show examples of EIS spectra recorded on the Ni/PANI (a), Ni_2Mo/PANI (b), and Ni_6Mo/PANI (c) electrocatalysts at an overpotential of −65 mV. The data are presented in the form of both Nyquist and Bode plots. The EIS spectra recorded on Ni/PANI (Fig. 3a) reveals the presence of only one time constant, while both NiMo/PANI spectra show the existence of two distinctive time constants. This is in agreement with EIS data obtained on other HER electrocatalysts [17,40]. In order to derive a physical picture of the electrode/electrolyte interface and the processes occurring at the electrode (catalyst) surface, experimental EIS data were modeled using non-linear least-squares fit analysis (NLLS) software [53] and electrical equivalent circuit (EEC). Three different EEC models presented in Fig. 4 have been used to fit the EIS response of the catalysts investigated [9,41,42,54,55]: (a) the one-time constant model (1T), (b) the two-time constant parallel model (2TP), and (c) the two-time constant serial model (2TS). In the absence of a response related to the hydrogen adsorption, the 1T model is used to describe a response of the HER on relatively smooth surfaces [52], surfaces containing narrow and wide cylindrical pores [55,56], or Pt–Co nano-particles supported on carbon [57]. The 2TP model (Fig. 4b), which represents a slightly modified model originally proposed by Armstrong and Henderson [58], has been used to describe the response of the HER on both porous [44,55,59] and smooth electrodes [60,61]. It reflects the response of a HER system characterized by two time constants, both of them related to the kinetics of the HER. It has been postulated that the first time constant (CPE_1–R_1, Fig. 4b) is related to the charge transfer kinetics, while the second time constant (CPE_2–R_2) is related to the hydrogen adsorption. It is important to note that in this case, both time constants change with overpotential. The 2TS model (Fig. 4c) has also been used to describe a response of the HER on porous electrodes [39,41,55]. Similarly to the 2TP model, it reflects the response of a HER system characterized by two time constants, but only one of them (CPE_1–R_1) is related to the kinetics of the HER. This time constant changes with overpotential. The second time constant (CPE_2–R_2) is related to the porosity of an electrode surface, and does not change with overpotential. Hence, from the discussion outlined above, it can be concluded that the suitability of a specific EEC to model experimental data can be used as a criterion

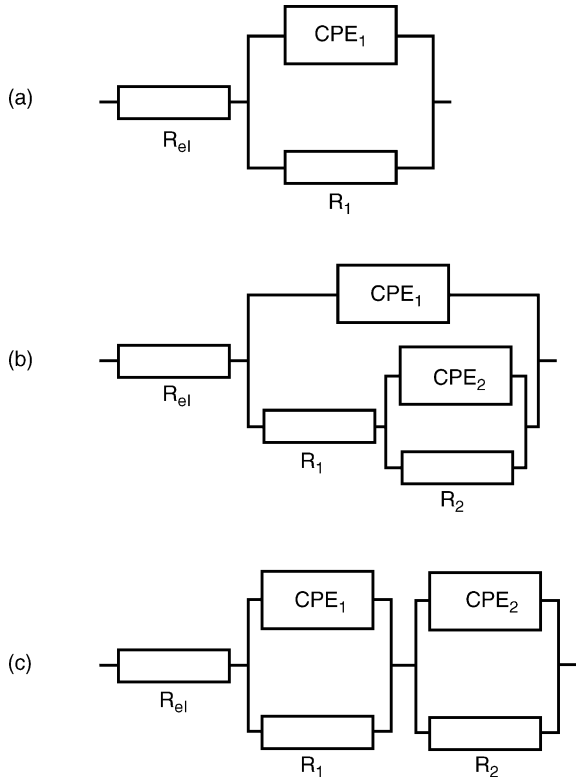

Fig. 4. EEC models used to explain the EIS response of the HER on nickel-based electrodes: (a) one-time constant model (1T), (b) two-time constant parallel model (2TP), and (c) two-time constant serial model (2TS).

to prescribe EEC parameters to the specific processes (i.e. charge transfer kinetics, surface porosity or hydrogen adsorption).

Fig. 3a shows that a very good agreement between the experimental (symbols) and simulated (lines) data is obtained when the 1T model is used to describe the EIS response of the Ni/PANI surface. An overpotential-dependent behavior of the EEC parameters (not shown here) revealed that with an increase in HER overpotential, the value of resistance, R_1, decreased, while the value of constant-phase-element, CPE_1, remained constant ($22 \pm 1\ \mu F\ s^{n-1}\ cm^{-2}$). Therefore, the time constant presented by the EEC in Fig. 4a represents a response of the HER kinetics on the Ni/PANI electrocatalyst, namely the charge transfer resistance, R_1, and double-layer capacitance, CPE_1. A fitting procedure showed that a better agreement between theoretical and experimental data was obtained when pure capacitance was replaced by a frequency-dependent constant phase element, CPE ($\Omega^{-1}\ s^n\ cm^{-2}$ or $F\ s^{n-1}\ cm^{-2}$). As already discussed in [17 and references therein], the use of a CPE is required due to a distribution of the relaxation times as a result of inhomogeneities present at the micro or nano (atomic/molecular) level, such as surface roughness/porosity, adsorption, diffusion, and non-uniform surface charge distribution.

For modeling of the two NiMo/PANI electrocatalysts, the suitability of both two-time-constant EEC models (Fig. 4b and c) was tested. However, only the 2TP model (Fig. 4b) yielded a very good agreement between the experimental and simulated data (Fig. 3b and c). In order to relate the two time constants to specific physical phenomena (charge-transfer kinetics,

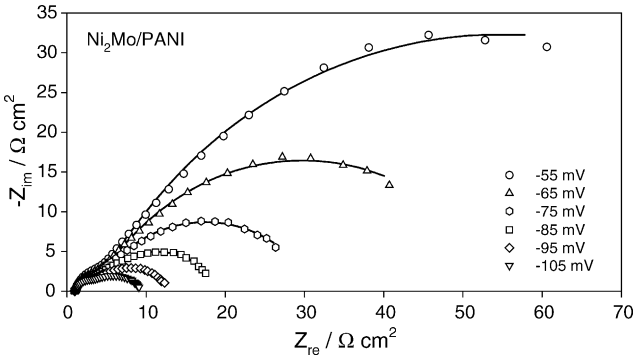

Fig. 5. Nyquist plot showing an EIS response of a Ni_2Mo/PANI electrode at various HER overpotentials. Symbols are experimental and solid lines are modeled data.

hydrogen adsorption, surface porosity), the dependence of each EEC parameter on applied overpotential should be carefully investigated. Fig. 5 shows a set of EIS spectra recorded on the Ni_2Mo/PANI electrode at various overpotentials. The figure demonstrates that the agreement between the experimental (symbols) and simulated (lines) data is very good at all the overpotentials investigated. The figure shows that with an increase in overpotential the diameter of both semicircles in the Nyquist plot decreases, thus indicating that both time constants change with overpotential. Studies of the HER on solid electrodes [39,41,55] have shown that when the radius of the high-frequency (HF) semicircle (smaller semicircle) is potential-independent, it can be related to the electrode surface porosity response, while the potential-dependent low-frequency (LF) semicircle (larger semicircle) is then related to the charge transfer resistance process and double layer capacitance. In such a case, a lower value time constant (HF constant) represents a response of surface pores, while a higher value time constant (LF constant) is related to the HER kinetics. On the other hand, when both semicircles, i.e. both time constants change with overpotential, as in Fig. 5, one of them is related to the response of hydrogen adsorbed on the electrode surface, while the other one represents the HER kinetics [44,55,59–61]. In such a case, the time constant related to the charge transfer resistance is usually much smaller than the time constant related to the adsorbed hydrogen. Hence, a response of the former appears in the high frequency region while the response related to the adsorbed hydrogen appears at low frequencies. Since the EIS spectra in Fig. 5 and EEC parameters obtained by modeling of all EIS spectra recorded on NiMo/PANI showed that both time constants change with overpotential, one can conclude that the 2TP EEC model (Fig. 4b) used to describe the AC response of the NiMo/PANi layers represents the response of a hydrogen adsorption process and charge transfer kinetics. Further, CPE_1 was shown to be relatively constant, with a very small standard deviation on both catalysts ($983 \pm 75\,\mu F\,s^{n-1}\,cm^{-2}$ for Ni_2Mo/PANI, and $197 \pm 42\,\mu F\,s^{n-1}\,cm^{-2}$ for Ni_6Mo/PANI). On the other hand, the value of resistance R_1 decreased rapidly with an increase in overpotential. Hence, on the basis of the overpotential behavior of these two parameters, it could be concluded that the first time constant (CPE_1–R_1) is related to the HER charge-transfer kinetics, namely to the response of double layer capacitance characterized by CPE_1, and HER charge transfer resistance characterized by R_1. Contrary to the behavior of CPE_1, the NLLS analysis demonstrated that the value of CPE_2 changed (increased) significantly with overpotential. At the same time, the value of R_2 decreased. This is a typical behavior related to the response of hydrogen adsorbed on an electrode surface, namely to the hydrogen adsorption pseudo-capacitance, CPE_2, and resistance, R_2 [44,55,59–61]. This EIS behavior is quite in consistence with the Tafel behavior and corresponding HER reaction mechanism discussed previously. As already determined from the Tafel measurements, the rds in the HER on the two NiMo/PANI catalysts represents the second reaction step (Heyrovsky), i.e. electrochemical desorption of adsorbed hydrogen ($M–H_{ads}$) to form molecular hydrogen (H_2). Hence, the first reaction step that represents adsorption of hydrogen (Volmer), $M–H_{ads}$, could be considered to be in equilibrium. Consequently, one could expect to record an AC response of the formed $M–H_{ads}$ layer, which was indeed confirmed by our EIS measurements as the appearance of the second time constant, CPE_2–R_2. On the other hand, the Tafel measurements (Fig. 2) showed that the rds on the Ni/PANI catalyst is the formation of the adsorbed hydrogen layer, $M–H_{ads}$, while the second reaction step (desorption) is then fast. Consequently, the absence of an EIS hydrogen absorption time constant (CPE_2–R_2) could be expected, as also confirmed by our EIS measurements. This demonstrates that although EIS and Tafel techniques are two quite different experimental techniques (ac versus DC), results obtained by both techniques are, at least qualitatively, comparable. Further, knowing that the HER proceeds in two steps (hydrogen adsorption and subsequent desorption to form molecular hydrogen [38–40]), it is then obvious from the presented EIS analysis that the overall rate of the HER is related to the sum of charge transfer, R_1, and hydrogen adsorption resistance, R_2 (except on Ni/PANI, in which case only R_1 is taken into account). Hence, combining these two resistances in series ($R_1 + R_2$) and applying Ohm's law it is possible to plot the semi-logarithmic dependence of the HER rate, $-\log(R_1 + R_2)$ versus applied overpotential, Fig. 6, and compare it to the Tafel plots presented in Fig. 2. Fig. 6 demonstrates that the EIS–Tafel curves follow the trend already seen on the DC polarization Tafel graph in Fig. 2. The Ni/PANI curve is characterized by a constant EIS–Tafel slope region, also yielding the lowest electrocatalytic HER activity. On the other hand, the Ni_2Mo/PANI layer shows the highest activity, followed by the Ni_6Mo/PANI layer. The shape of both EIS–Tafel curves is very similar to the shape seen in Fig. 2, showing the presence of two Tafel regions, with a transition point between −150 mV and −200 mV.

Besides the information on the kinetics of the HER and hydrogen adsorption, EIS results can also be used to estimate the real surface area of electrocatalytic layers using a value of double layer capacitance. This is important since, by knowing the real electrochemically active area of the catalyst, it is possible to determine its intrinsic activity in the HER, eliminating the effect of surface roughness. Taking that the average double layer capacitance of a smooth metal surface is $20\,\mu F\,cm^{-2}$ [62,63], the real

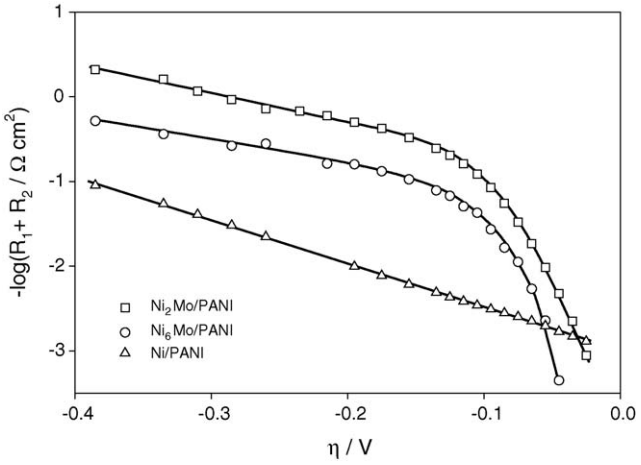

Fig. 6. EIS–Tafel curves obtained from impedance data. $R_1 + R_2$ represents the total resistance to the HER.

surface area can be calculated as $A_{real} = C_{DL}/20\,cm^2$, and then the roughness factor, that characterizes the real-to-geometrical surface area ratio, can be calculated as $\sigma = A_{real}/A_{geometric}$. As previously discussed, the double layer capacitance of the studied layers is described by the constant phase element CPE_1 and its exponent n_1. However, although the value of parameter n_1 is close to unity (0.883 ± 0.005 for Ni/PANI, 0.854 ± 0.048 for Ni_2Mo/PANI, and 0.934 ± 0.060 for Ni_6Mo/PANI), its small deviation indicates the presence of surface inhomogeneities, most likely in terms of charge distribution. However, the actual value of the double layer capacitance, C_{DL}, can be conveniently calculated using an equation originally proposed by Brug et al. [64] and later used by many researchers [8,9,40–42,57,62,65], $C_{DL,i} = [CPE_i(R_{el}^{-1} + R_i^{-1})^{(n-1)}]^{1/n}$. Mean values of the double layer capacitance, together with the corresponding standard deviation and calculated roughness factor for the investigated layers, are presented in Table 3. The table shows that the double layer capacitance standard deviation is rather small, i.e. the value of the double layer capacitance remains very constant in the whole overpotential region investigated. This indicates that the accessibility of the catalyst surface to the electrolyte remains constant, thus dismissing the possibility of surface blockage by produced molecular hydrogen. This also confirms that the change in Tafel slope on the NiMo/PANI layers (Figs. 2 and 6) is not a result of a decreased surface area but formation of hydrides, which was already discussed previously in the text.

Table 3
Double layer capacitance (normalized to the geometric area of the electrode) and corresponding surface roughness values for the investigated catalytic coatings calculated from the EIS data obtained in the entire overpotential region investigated. Results for a control-catalyst (Ni-control) are also presented for comparison

Catalyst	C_{DL} (F cm^{-2})	σ
Ni-control	$(6.4 \pm 0.3) \times 10^{-5}$	3.2
Ni/PANI	$(1.8 \pm 0.1) \times 10^{-4}$	9.0
Ni_2Mo/PANI	$(7.1 \pm 1.2) \times 10^{-3}$	355
Ni_6Mo/PANI	$(1.2 \pm 0.2) \times 10^{-3}$	60

Table 4
Current density at overpotential of −150 mV obtained from Tafel plots (Fig. 2) normalized to the real surface area of the catalyst. The most right column represents an inverse of the kinetic resistance normalized to the true surface area of the electrode obtained from Fig. 6. Results for a control-catalyst (Ni-control) are also presented for comparison

Catalyst	Tafel j/σ at −150 mV (μA cm^{-2})	EIS $10^4/(R_1 + R_2)\sigma$ at −150 mV (Ω^{-1} cm^{-2})
Ni-control	−8.4	0.6
Ni/PANI	−23.1	6.5
Ni_2Mo/PANI	−27.6	9.4
Ni_6Mo/PANI	−59.7	17.1

The data in Table 3 also outlines values of the surface roughness for each of the surfaces studied. This allows us to evaluate the relative intrinsic catalytic activity of the investigated catalysts, by eliminating the effect of surface area. For this purpose, the Tafel plots presented in Figs. 2 and 6 were normalized to the true surface area by dividing the curves by the corresponding surface roughness factor. Table 4 lists the normalized current density and inverse kinetic resistance values recorded at −150 mV for the electrocatalysts used in research. Although previous data based on the geometric area (Table 2) confirmed that Ni_2Mo/PANi yields the highest *overall* electrocatalytic activity in the HER, the data in Table 4 shows that Ni_6Mo/PANI yields the highest *intrinsic* activity in the HER, approximately seven times higher than the Ni-control surface. The other interesting observation is that the Ni/PANI surface is almost three times more active than the Ni-control surface. Since in both cases the same electrocatalytic material was used (Ni), the increased electrocatalytic activity of the Ni layer obtained by electrodeposition of Ni in the presence of PANI on the substrate surface could be explained only by an increased number of electrochemically active sites present on the Ni/PANI surface. A catalyst/support interaction could be dismissed as a contributing factor since only traces of PANI residues are present on the catalyst's surface.

The increased intrinsic activity of the bicomponent NiMo catalysts in comparison to pure Ni is in accordance with literature [17,22]. It is well known that the HER electrocatalytic activity of Ni can be improved by the addition of a second metal into the alloy. A general conclusion found in literature is that the intrinsic catalytic activity for the HER is related to the electronic structure of metals, although any explicit and comprehensive explanation has not yet been given. The theoretical approach in explaining the HER activity of alloy catalysts is even more complex, and several theories have been proposed. A well-known 'spillover' process in heterogeneous catalysis has also been used to interpret the synergism of transition metal-based HER alloys, more specifically NiMo [22]. In this theory, simple cooperative functioning of the alloy components is mediated via rapid intra- and inter-particle surface diffusion of H ad-atoms. The authors essentially rule out any relationship between the electronic interactions among NiMo alloy components and observed synergy. On the other hand, Jaksic et al. [66,67] take into account solely the influence of electronic density (distribution) on the corresponding electrocatalytic HER activity of transition metal-based alloys. They discuss both the hydrogen evolution activity and

catalyst stability on the basis of the Engel–Brewer valence-bond theory, as a generalized Lewis acid–base reaction model. The theory proposed by this research group has been supported by a number of experimental studies related to the HER electrocatalysis [60,67,68]. Another theory related to the synergism of HER bimetallic catalysts has been proposed by Ezaki et al. [18–20]. They also based their explanation on the electronic structure of alloys. However, the main difference between the latter two theories is in the direction of electron transfer between constituting atoms in an alloy and its effect on the respective Fermi levels of the components. An experimental support related to the direction of electron transfer postulated by Jaksic et al. can be found in recent papers published by Wieckowski et al. [69–72] (NMR and XPS studies), while UPS experiments published by Oelhafen et al. [73–75] give a strong support to Ezaki's theory. Ezaki et al. [18–20] have also postulated that an increase in the HER electrocatalytic activity coincides with an increase in electron density around the more electronegative constituent of an alloy (Ni in our case). On the other hand, Jaksic's theory predicts an *optimum* electron density for the best HER electrocatalytic activity of an alloy, and does not recognize specific surface sites (in terms of alloy constituents) as hydrogen active sites. Similar conclusions have been reported by Kawashima et al. [45] who have shown that the optimum electron configuration corresponds to the situation of a nearly filled d-orbital. The d-band vacancy of Ni in NiMo alloys decreases with the addition of Mo and becomes nearly zero at ca. 11 at.% Mo. This composition would, hence, give the best activity in the HER, which is in good agreement with results in [45], and also results obtained on NiMo metal ultra-fine particles [76]. Our results on Ni_6Mo/PANI (14.3 at.% Mo), Table 4, also support the assumption that the highest activity in the HER can be expected at a composition around 11 at.% Mo. With an increase in Mo content to ca. 33 at.% (Ni_2Mo/PANI), the intrinsic activity of the alloy decreases to ca. 50% of the value obtained on Ni_6Mo/PANI (Table 4). Taking into account the above theories and considering the HER reaction mechanism [38–40], we believe that the influence of electronic structure on the catalytic activity of bimetallic catalysts plays one of the major roles in the kinetics of the HER, but the surface diffusion cannot be completely excluded as a contributing factor. This opinion is logical if we consider the HER reaction mechanism [38–40], from which it is obvious that the kinetics of the HER depends on both the electron-transfer rate and the strength of the M–H_{ads} bond, which both, in turn, depend on the d-electron density at the Fermi level. This opinion is supported by the experimental results of Wieckowski et al. [69–72] who have recently shown that alloying Pt with Ru induces major changes in the core-level binding energies of chemisorbed carbon monoxide (CO). Schlapka et al. [77] have also recently shown that the electronic effect plays the major role in the adsorption strength of CO on up to four monolayers of Pt deposited on Ru, after which a surface strain effect starts to predominate.

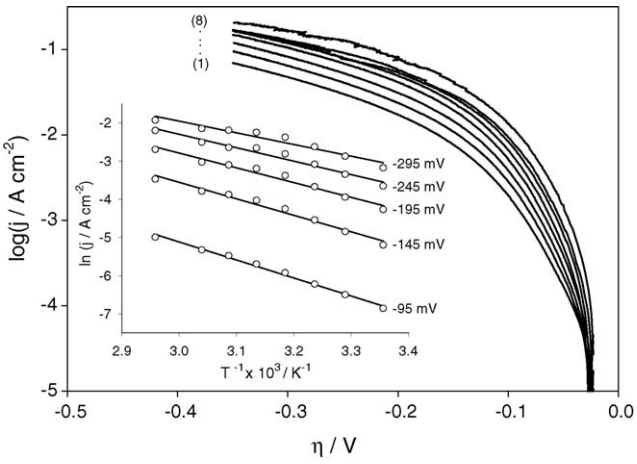

Fig. 7. Linear Tafel polarization curves recorded on the Ni_2Mo/PANI electrocatalysts at (1) 298 K, (2) 304 K, (3) 309 K, (4) 314 K, (5) 319 K, (6) 323 K, (7) 329 K, and (8) 338 K. The curves were corrected for the IR-drop; scan rate = 0.5 mV s^{-1}. The inset shows an Arrhenius-type semi-logarithmic dependence of current density on inverse temperature obtained at several selected overpotentials.

3.4. Activation energy

In order to evaluate the effect of temperature on the kinetics of the HER on the investigated PANI-based layers, DC linear polarization (Tafel) measurements were done for a wide temperature range, from 298 K to 338 K. Fig. 7 shows a set of Tafel curves recorded on the Ni_2Mo/PANI surface at various temperatures. With an increase in temperature, the current density at a fixed overpotential also increases (an average of 5.2 times in the whole potential region by going from 298 K to 338 K). The inset in Fig. 7 demonstrates that this increase is linear in a semi-logarithmic plot, which is in accordance with the Arrhenius law [57], $\ln j_{\eta=\text{const}} = -E_{act}/TR + \ln A_0$, where E_{act} (J mol^{-1}) represents the apparent activation energy for the HER, and A_0 (A cm^{-2}) is the pre-exponential factor. Thus, from the slope of the line, the apparent activation energy value could be calculated. Table 5 lists apparent activation energy values calculated

Table 5
Apparent activation energy values calculated at various overpotentials. The most right column outlines a *R*-squared coefficient for a E_{act} vs. η dependence for each PANI-based catalyst

Catalyst	E_{act} (kJ mol^{-1})						$dE_{act}/d\eta$ (kJ mol^{-1} V^{-1})	R^2
	0[a]	95[a]	145[a]	195[a]	245[a]	295[a]		
Ni/PANI	73.4	69.7	66.1	63.2	62.6	59.8	46.7	0.9805
Ni_2Mo/PANI	45.8	39.3	36.0	32.2	29.2	25.4	68.9	0.9995
Ni_6Mo/PANI	44.8	39.1	34.5	30.1	26.2	25.4	70.9	0.9807

[a] η (mV).

at several selected overpotentials. The trend seen agrees well with the trend obtained from the Tafel and EIS measurements (Tables 2–4). The two bimetallic NiMo/PANI catalysts show a higher activity (lower activation energy) than the Ni/PANI catalyst. The corresponding apparent activation energy values on the NiMo/PANI surfaces are nearly the same, which indicates that the HER reaction mechanism on these two surfaces follows the same path, as already concluded from the Tafel and EIS measurements discussed previously in the text. The values obtained at zero overpotential are also very close to those usually postulated for HER occurring through the Heyrovsky mechanism [57]. Savadogo et al. [57] obtained values ranging from 36 kJ mol^{-1} to 56 kJ mol^{-1} on Pt–Co supported on carbon at zero overpotential, while Giz et al. [78] reported a value of 39 kJ mol^{-1} on NiZn. A higher value (62 kJ mol^{-1}) was reported on NiFeZn [79]. From results reported in [80], activation energy values of 39 kJ mol^{-1} and 49 kJ mol^{-1} could be calculated on NiAl catalysts containing 20 at.% and 30 at.% Al, respectively. According to the electrochemical theory [38], with an increase in overpotential one can expect to see a linear decrease in activation energy. The analysis of the data in Table 5 showed that a very good agreement between the theory and experimental data was indeed observed on all the three surfaces studied, as demonstrated by a high value of the regression (determination) coefficient. The slope of the E_{act} versus η line, which is also presented in the table, shows the influence of overpotential on the resulting change in apparent activation energy. Considering that certain overpotential is needed in order to produce hydrogen in a hydrogen generator, a higher value of the slope indicates higher electrocatalytic activity of the catalyst. Hence, the two bimetallic catalysts again demonstrate superior behavior over the Ni/PANI catalyst, which is quite in accordance to the behavior seen in Figs. 2 and 6.

4. Conclusions

Electrocatalytic activity of Ni and NiMo layers produced by electrodeposition on/in a preformed PANI layer (matrix) was investigated in the hydrogen evolution reaction (HER). The influence of alloying Ni by left-hand side transition metal, Mo, on the electrocatalytic activity in the HER was also investigated.

It was shown that by using PANI an increase in surface roughness of the resulting metallic catalytic layers could be obtained. In the presence of PANI on the glassy carbon substrate, 3D porous metallic Ni and NiMo layers were produced. The morphology of the layers was characterized as spherical/globular particles of an average diameter of 3 μm.

It was also clearly demonstrated that alloying Ni with Mo results in an increased electrocatalytic activity in the HER when compared to pure Ni. Two effects were found to be responsible for the observed behavior; an increase in surface roughness and intrinsic activity of the material. Both bimetallic layers were found to offer a higher electrocatalytic activity than Ni/PANI, which is predominantly due to an increased surface roughness. Ni_2Mo/PANI was found to yield the highest *overall* electrocatalytic activity among the investigated materials, while Ni_6Mo/PANI expressed the highest *intrinsic* electrocatalytic activity. The latter was explained on the basis of the modification of the electron density in the d-shell upon alloying Ni with Mo in a way that favors the HER kinetics. It was also shown that the two NiMo/PANI catalysts offer considerably lower activation energy in the HER than the Ni/PANI layer, which is also a consequence of better intrinsic properties of the bimetallic materials.

DC linear polarization and AC electrochemical impedance spectroscopy measurements allowed us to determine the mechanism and kinetics of the HER. It was shown that the kinetics of the HER on Ni/PANI is controlled by the Volmer reaction step as the rds (electrochemical adsorption of hydrogen to form Ni–H_{ads}), while the Heyrovsky step (electrochemical desorption of hydrogen to form H_2) was shown to be the rds on the two bimetallic NiMo/PANI catalysts.

Acknowledgements

Grateful acknowledgment is made to Fonds québécois de la recherche sur la nature et les technologies and the Natural Science and Engineering Research Council of Canada for support of this research.

References

[1] S. Dun, Int. J. Hydrogen Energy 27 (2002) 235.
[2] T. Hijikata, Int. J. Hydrogen Energy 27 (2002) 115.
[3] P. Kruger, Int. J. Hydrogen Energy 25 (2000) 395.
[4] C. Mitsugi, A. Harumi, F. Kenzo, Int. J. Hydrogen Energy 23 (1998) 159.
[5] M. Kondoh, N. Yokoyama, C. Inazumi, S. Maezawa, N. Fujiwara, Y. Nishimura, K. Oguro, H. Takenaka, J. New Mater. Electrochem. Syst. 3 (2000) 61.
[6] P. Millet, F. Andolfatto, R. Durand, Int. J. Hydrogen Energy 21 (1996) 87.
[7] R. Steinberger-Wilckens, J. Linnemann, 207th Meeting of the Electrochemical Society, Quebec City, Que., Canada, 2005.
[8] P. Los, A. Rami, A. Lasia, J. Appl. Electrochem. 23 (1993) 135.
[9] C. Hitz, A. Lasia, J. Electroanal. Chem. 500 (2001) 213.
[10] S. Tanaka, N. Hirose, T. Tanaki, Int. J. Hydrogen Energy 25 (2000) 481.
[11] W. Hu, Int. J. Hydrogen Energy 25 (2000) 111.
[12] M.H. Miles, M.A. Thomason, J. Electrochem. Soc. 123 (1976) 1459.
[13] B.E. Conway, J.O'M. Bockris, J. Chem. Phys. 26 (1957) 532.
[14] L.I. Krishtalik, in: P. Delahay, C. Tobias (Eds.), Advances in Electrochemistry and Electrochemical Engineering, vol. 7, Interscience, New York, 1970.
[15] S. Trasatti, J. Electroanal. Chem. 39 (1972) 163.
[16] S. Trasatti, J. Chem. Soc. Faraday Trans. 68 (1972) 229.
[17] E. Navarro-Flores, Z. Chong, S. Omanovic, J. Mol. Catal. A: Chem. 226 (2005) 179.
[18] H. Ezaki, M. Morinaga, S. Watanabe, Electrochim. Acta 38 (1993) 557.
[19] H. Ezaki, M. Morinaga, S. Watanabe, J. Saito, Electrochim. Acta 39 (1994) 1769.
[20] H. Shibutani, T. Higashijima, H. Ezaki, M. Morinaga, K. Kikuchi, Electrochim. Acta 43 (1998) 3235.
[21] M.M. Jaksic, Electrochim. Acta 45 (2000) 4085;
M.M. Jaksic, Solid State Ionics 136/137 (2000) 733.
[22] J.G. Highfield, E. Claude, K. Oguro, Electrochim. Acta 44 (1999) 2805.
[23] K. Bouzek, K.-M. Mangold, K. Jüttner, Electrochim. Acta 46 (2000) 661.
[24] K. Bouzek, K.-M. Mangold, K. Jüttner, J. Appl. Electrochem. 31 (2001) 501.

[25] H. Laborde, J.-M. Leger, C. Lamy, J. Appl. Electrochem. 24 (1994) 1019.
[26] W.T. Napporn, H. Laborde, J.-M. Leger, C. Lamy, J. Electroanal. Chem. 404 (1996) 153.
[27] M.J. Croissant, T. Napporn, J.-M. Leger, C. Lamy, Electrochim. Acta 43 (1998) 2447.
[28] P.J. Kulesza, M. Matczak, A. Wolkiewicz, B. Grzybowska, M. Galkowski, M.A. Malik, A. Wieckowski, Electrochim. Acta 44 (1999) 2131.
[29] A. Zouaoui, O. Stéphan, A. Ourari, J.-C. Moutet, Electrochim. Acta 46 (2000) 49.
[30] M.T. Giacomini, E.A. Ticianelli, J. McBreen, M. Balasubramanian, J. Electrochem. Soc. 148 (2001) A323.
[31] C. Coutanceau, J.J. Croissant, T. Napporn, C. Lamy, Electrochim. Acta 46 (2000) 579.
[32] C.C. Chen, C.S.C. Bose, K. Rajeshwar, J. Electroanal. Chem. 350 (1993) 161.
[33] A. Jukic, M. Metikos-Hukovic, Electrochim. Acta 48 (2003) 3929.
[34] M. Grzeszczuk, P. Poks, Electrochim. Acta 45 (2000) 4171.
[35] M.M. Saleh, J. Appl. Electrochem. 30 (2000) 939.
[36] L.M. Abrantes, J.P. Correia, Electrochim. Acta (2000) 4179.
[37] B. Pfeiffer, A. Thyssen, J.W. Schultze, J. Electroanal. Chem. 260 (1989) 393.
[38] Southampton Electrochemistry Group, Instrumental Methods in Electrochemistry, Wiley, New York, 1985.
[39] B. Borresen, G. Hagen, R. Tunold, Electrochim. Acta 47 (2002) 1819.
[40] E. Ndzebet, O. Savadogo, Int. J. Hydrogen Energy 20 (1995) 635.
[41] B. Losiewicz, A. Budniok, E. Rowinski, E. Lagiewka, A. Lasia, Int. J. Hydrogen Energy 29 (2004) 145.
[42] R.K. Shervedani, A. Lasia, J. Electrochem. Soc. 144 (1997) 2652.
[43] A. Krolikowski, A. Wiecko, Electrochim. Acta 47 (2002) 2065.
[44] R. Simpraga, G. Tremiliosi-Filho, S.Y. Qian, B.E. Conway, J. Electroanal. Chem. 424 (1997) 141.
[45] A. Kawashima, E. Akiyama, H. Habazaki, K. Hashimoto, Mater. Sci. Eng. A226–A228 (1997) 905.
[46] A. Rami, A. Lasia, J. Appl. Electrochem. 22 (1992) 376.
[47] J.G. Highfield, K. Oguro, B. Grushko, Electrochim. Acta 47 (2001) 465.
[48] N. Krstajic, S. Trasatti, J. Appl. Electrochem. 28 (1998) 1291.
[49] C.A. Marozzi, A.C. Chialvo, Electrochim. Acta 46 (2001) 861.
[50] M.C. Taveres, S.A.S. Machado, L.H. Mazo, Electrochim. Acta 46 (2001) 4359.
[51] K.R. Christmann, in: Z. Paal, P.G. Menon (Eds.), Hydrogen Effects in Catalysis, Marcel Dekker, 1988 (Chapter 1).
[52] M. Metikos-Hukovic, A. Jukic, Electrochim. Acta 45 (2000) 4159.
[53] B.A. Boukamp, Equivalent Circuit Users Manuel, Report CT88/265/128, University of Twente, Department of Chemical Technology, The Netherlands, 1989.
[54] J. Panek, A. Serek, A. Budniok, E. Rowinski, E. Lagiewka, Int. J. Hydrogen Energy 28 (2002) 169.
[55] L. Birry, A. Lasia, J. Appl. Electrochem. 34 (2004) 735.
[56] P. Elumalai, H.N. Vasan, N. Munichandraiah, S.A. Shivashankar, J. Appl. Electrochem. 32 (2002) 1005.
[57] O. Savadogo, E. Ndzebet, Int. J. Hydrogen Energy 26 (2001) 213.
[58] R.D. Armstron, M. Henderson, J. Electroanal. Chem. 39 (1972) 81.
[59] E.B. Castro, M.J. de Giz, E.R. Gonzalez, J.R. Vilche, Electrochim. Acta 42 (1997) 951.
[60] J.M. Jaksic, M.V. Vojnovic, N.V. Krstajic, Electrochim. Acta 45 (2000) 4151.
[61] F. Rosalbino, G. Borzone, E. Angelini, R. Raggio, Electrochim. Acta 48 (2003) 3939.
[62] L. Chen, A. Lasia, J. Electrochem. Soc. 139 (1992) 3214.
[63] S. Trasatti, O.A. Petrii, Pure Appl. Chem. 63 (1991) 711.
[64] G.J. Brug, A.L.G. Van Der Eeden, M. Sluyters-Rehbach, J.H. Sluyters, J. Electroanal. Chem. 176 (1984) 275.
[65] R.K. Shervedani, A. Lasia, J. Appl. Electrochem. 29 (1999) 979.
[66] M.M. Jaksic, Int. J. Hydrogen Energy 26 (2001) 559.
[67] M.M. Jaksic, C.M. Lacnjevac, B.N. Grgur, N.V. Krstajic, J. New Mater. Electrochem. Syst. 3 (2000) 169.
[68] N.V. Krstajic, B.N. Grgur, N.S. Mladenovic, M.V. Vojnovic, M.M. Jaksic, Electrochim. Acta 42 (1997) 323.
[69] P.K. Babu, H.S. Kim, A. Wieckowski, E. Oldfield, J. Phys. Chem. B 107 (2003) 7595.
[70] Y.Y. Tong, H.S. Kim, P.K. Babu, P. Waszczuk, A. Wieckowski, E. Oldfield, J. Am. Chem. Soc. 124 (2002) 468.
[71] C. Vericat, M. Wakisaka, R. Haasch, P.S. Bagus, A. Wieckowski, J. Solid State Electrochem. 8 (2004) 794.
[72] A. Wieckowski, personal communication.
[73] P. Oelhafen, E. Hauser, H.J. Guntherodt, K.H. Bennemann, Phys. Rev. Lett. 43 (1979) 1134.
[74] P. Oelhafen, E. Hauser, H.J. Guntherodt, Solid State Commun. 35 (1980) 1017.
[75] J. Kubler, K.H. Bennemann, R. Lapka, F. Rosel, P. Oelhafen, H.J. Guntherodt, Phys. Rev. B 23 (1981) 5176.
[76] H. Ezaki, T. Nambu, M. Morinaga, M. Udaka, K. Kawasaki, Int. J. Hydrogen Energy 21 (1996) 877.
[77] A. Schlapka, M. Lischka, A. Gross, U. Kasberger, P. Jakob, Phys. Rev. Lett. 91 (2003) paper 016101.
[78] M.J. Giz, S.A.S. Machado, L.A. Avaca, E.R. Gonzalez, J. Appl. Electrochem. 22 (1992) 973.
[79] M.J. Giz, S.C. Bento, E.R. Gonzalez, Int. J. Hydorgen Energy 25 (2000) 621.
[80] R.P. Simpraga, B.E. Conway, Electrochim. Acta 43 (1998) 3045.